




Multifunctional properties of microwave assisted CuO/Cu₂O-ZnO mixed metal oxide nanocomposites

Ravi Kumar^{1,3}, Kuldeep Kumar^{1,3,*} , Saurabh Sharma^{1,3}, Nikesh Thakur^{2,3}, and Naveen Thakur^{2,3,*}

¹Department of Chemistry, Career Point University, Hamirpur, H.P. 176041, India

²Department of Physics, Career Point University, Hamirpur, H.P. 176041, India

³Centre for Nano-Science and Technology, Career Point University, Hamirpur, H.P. 176041, India

Received: 3 March 2023

Accepted: 20 May 2023

Published online:
31 May 2023

© The Author(s), under exclusive licence to Springer Science+Business Media, LLC, part of Springer Nature 2023

ABSTRACT

The bimetallic CuO/Cu₂O-ZnO nanocomposites (NCs) were synthesized using *Ipomoea carnea* leaf extract. The Cu and Zn were mixed in ratios of 90:10, 80:20, 70:30, and 60:40, and the mixture was heated under controlled microwave conditions (2.45 GHz and 700 W). Various spectroscopic techniques were used to characterize the synthesized samples. The XRD patterns confirmed crystallinity, and the size of the synthesized CuO/Cu₂O-ZnO NCs was estimated to be in the range of 7–24 nm. SEM images showed well-defined star, spherical, and flower-like shapes, while TEM analysis revealed the size of the NCs to be between 8–50 nm. The presence of elemental and organic compositions was confirmed by EDX and FTIR analysis. The energy band gaps ranged between 1.47–2.9 eV, while the stability of the CuO/Cu₂O-ZnO NCs was found to be in the range of – 15.7 to – 26.9 mV based on zeta potential values. XPS analysis confirmed the purity of the synthesized materials. Antibacterial activity against human pathogens, *Staphylococcus aureus*, *Escherichia coli*, and *Bacillus subtilis*, was demonstrated using the well diffusion method. Additionally, the 90:10 CuO/Cu₂O-ZnO NCs exhibited high photocatalytic degradation efficiency for methyl orange (96.45%) and methylene blue (98.96%) dyes within 45 min. However, the maximum antioxidant activity (99.77%) was observed in the case of 60:40 CuO/Cu₂O-ZnO NCs.

1 Introduction

The biosynthesis of nanoparticles plays a unique role in maintaining financial growth while reducing ecological loads, using phytochemicals or living organisms from plant resources [1, 2]. Among

nanoparticles, transition metal oxide nanoparticles are essential for various applications such as photocatalysis, antioxidation, and antibacterial activities [3]. While physical and chemical methods are expensive, toxic, and harmful to both human health and the environment, research has been conducted

Address correspondence to E-mail: kuldeep.sharma.753@gmail.com; naveenthakur2327@gmail.com

Scheme 1 The schematic diagram for the synthesis of CuO/Cu₂O-ZnO nanocomposites

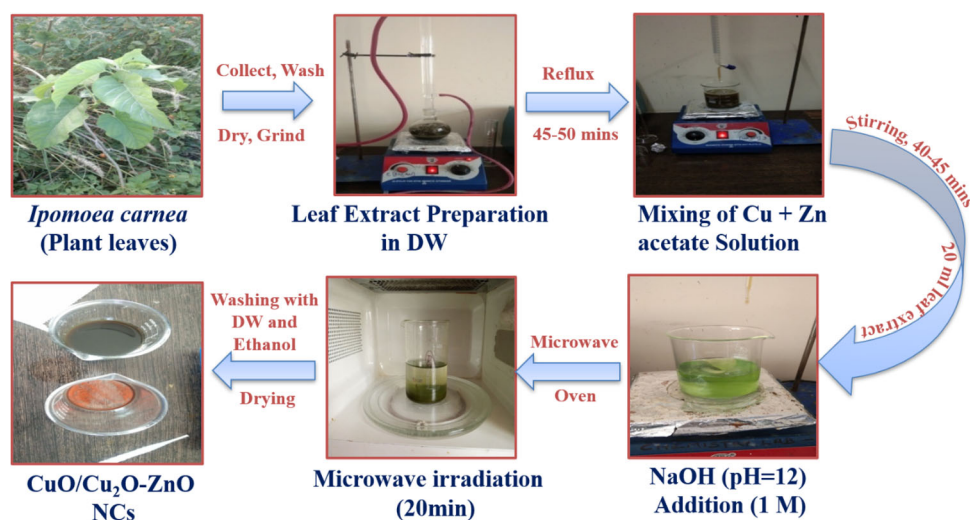
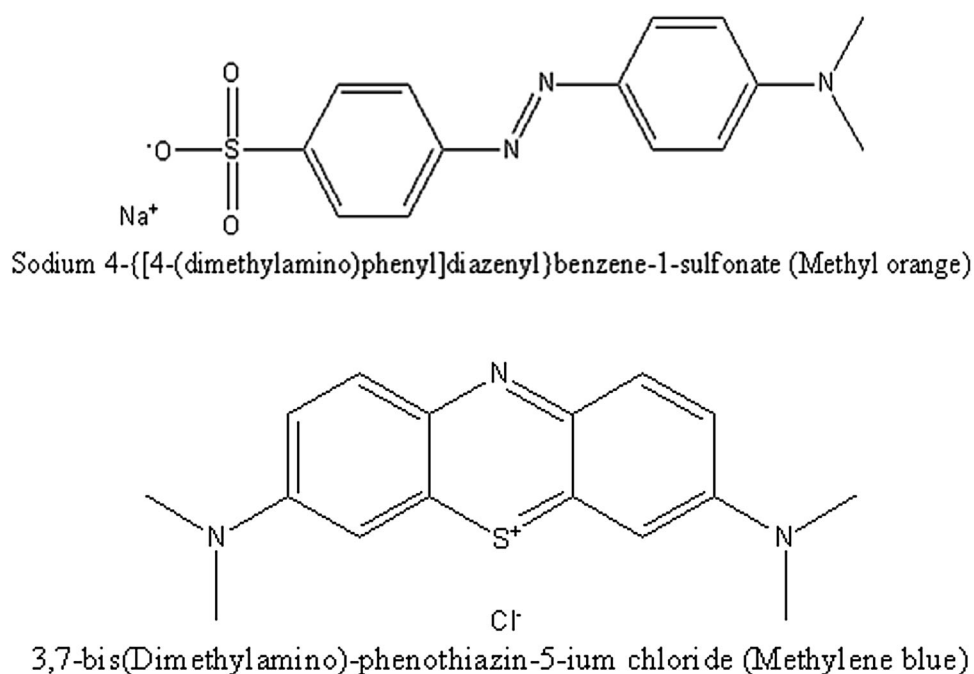


Fig. 1 Organic structures of methyl orange (MO) and methylene blue (MB)



for the last three decades to develop new techniques to cope with these issues. Indeed, green synthesis provides a good alternative route to synthesize nanoparticles, particularly for biological and pharmaceutical uses.

Metal oxide nanoparticles are useful in various applications such as sensors, photocatalysts, UV protection, drug carriers, cosmetics, antioxidant, and antibacterial agents due to their unique properties [4, 5]. Zinc oxide (ZnO) is a n-type semiconductor with a wide bandgap of ~ 3.3 eV, high exciton binding energy of ~ 60 meV, wurtzite crystal structure, and piezoelectric properties [6–8]. Copper oxide

(CuO) is another commonly used p-type semiconductor with a low energy bandgap of ~ 1.2 eV, monoclinic structure, excellent chemical stability, environmental friendliness, and anti-inflammatory and antibacterial activities [9–11]. This semiconductor material has been mainly applied in photo-electrochemical water reduction, gas sensing, catalytic activity, solar hydrogen production, photo-degradation reactions, and photovoltaic applications [12, 13]. Recently, copper oxide (CuO) and zinc oxide (ZnO) have gained significant interest in scientific research and have varied scopes in modern life due to their unique and promising properties.

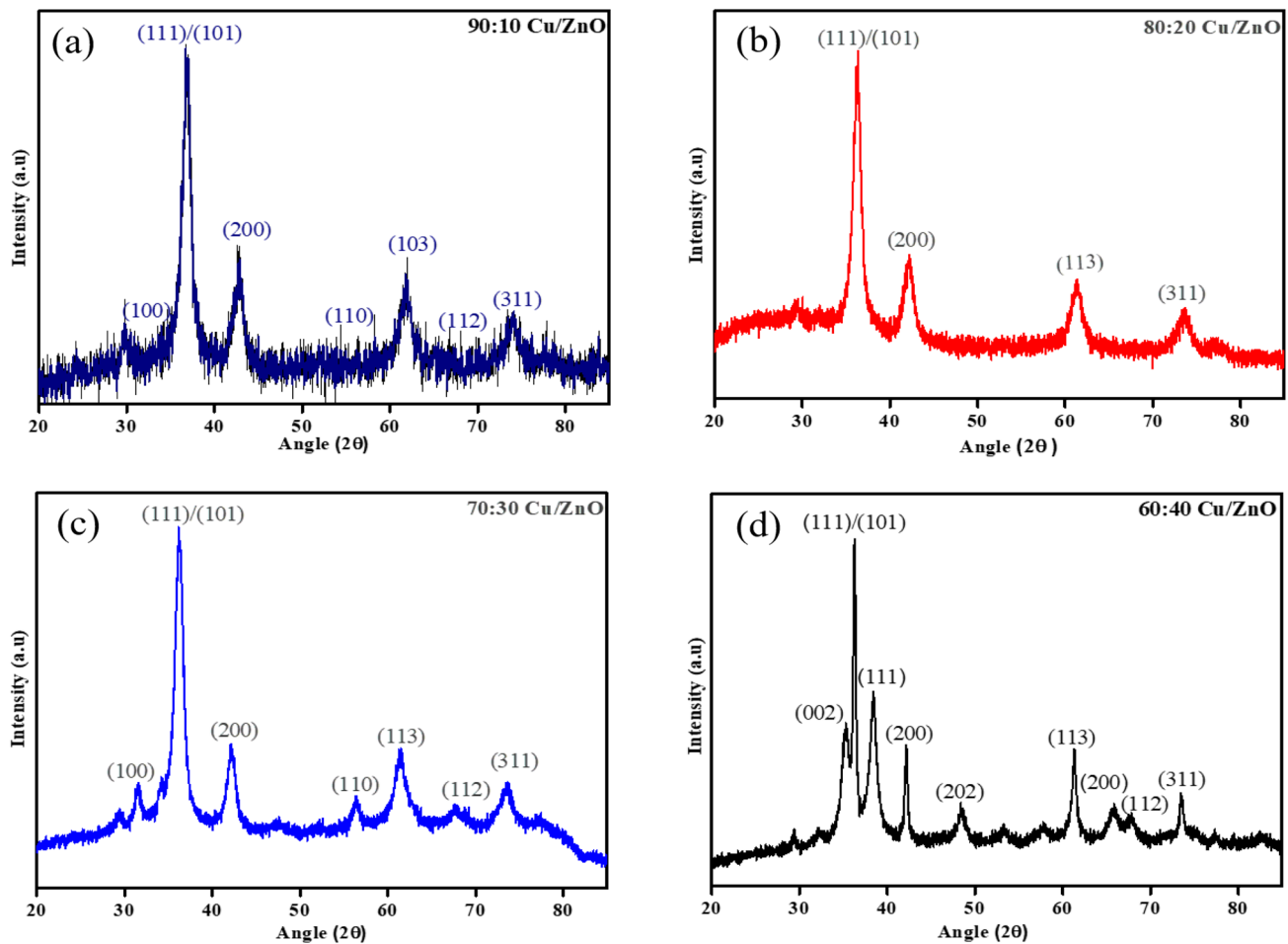


Fig. 2 The XRD patterns of the **a** 90:10, **b** 80:20, **c** 70:30, and **d** 60:40 CuO/Cu₂O-ZnO nanocomposites

Table 1 Structural parameters, *D*, *d*, δ and ϵ of various synthesized CuO/Cu₂O-ZnO nanocomposites

CuO/Cu ₂ O-ZnO	Crystallite size (<i>D</i>) (nm)	Interplanar Spacing (<i>d</i>) (Å)	Dislocation density (δ) (nm ⁻²)	Strain (ϵ)
90:10	7	0.2431	0.0205	0.0155
80:20	7	0.2397	0.0187	0.0150
70:30	7	0.2392	0.0200	0.0156
60:40	24	0.2393	0.0017	0.0046

NCs are important materials in nanotechnology that have attracted great attention due to their unique properties, which are not found in conventional composites. Metal oxide nanocomposites have been identified as appropriate alternatives to overcome the limitations of nanoparticle agglomeration [14, 15]. Specifically, transition metal oxide nanocomposites, such as CuO and ZnO, have received significant attention in scientific research due to their exclusive properties. One primary disadvantage of nanoparticles is their small size, which limits their use in a

wide range of applications due to agglomeration that decreases their surface area, activity, and efficiency. Researchers have developed a variety of metal oxide nanocomposites to increase surface area and improve the photocatalytic, antibacterial, antifungal, and antioxidant properties of the materials [16–19]. Different methods have been developed to prepare the distinct metal oxide nanocomposites, including microwave-irradiation, sol-gel, chemical vapor deposition, co-precipitation, and mechanical alloying. Among them, the microwave-irradiation in

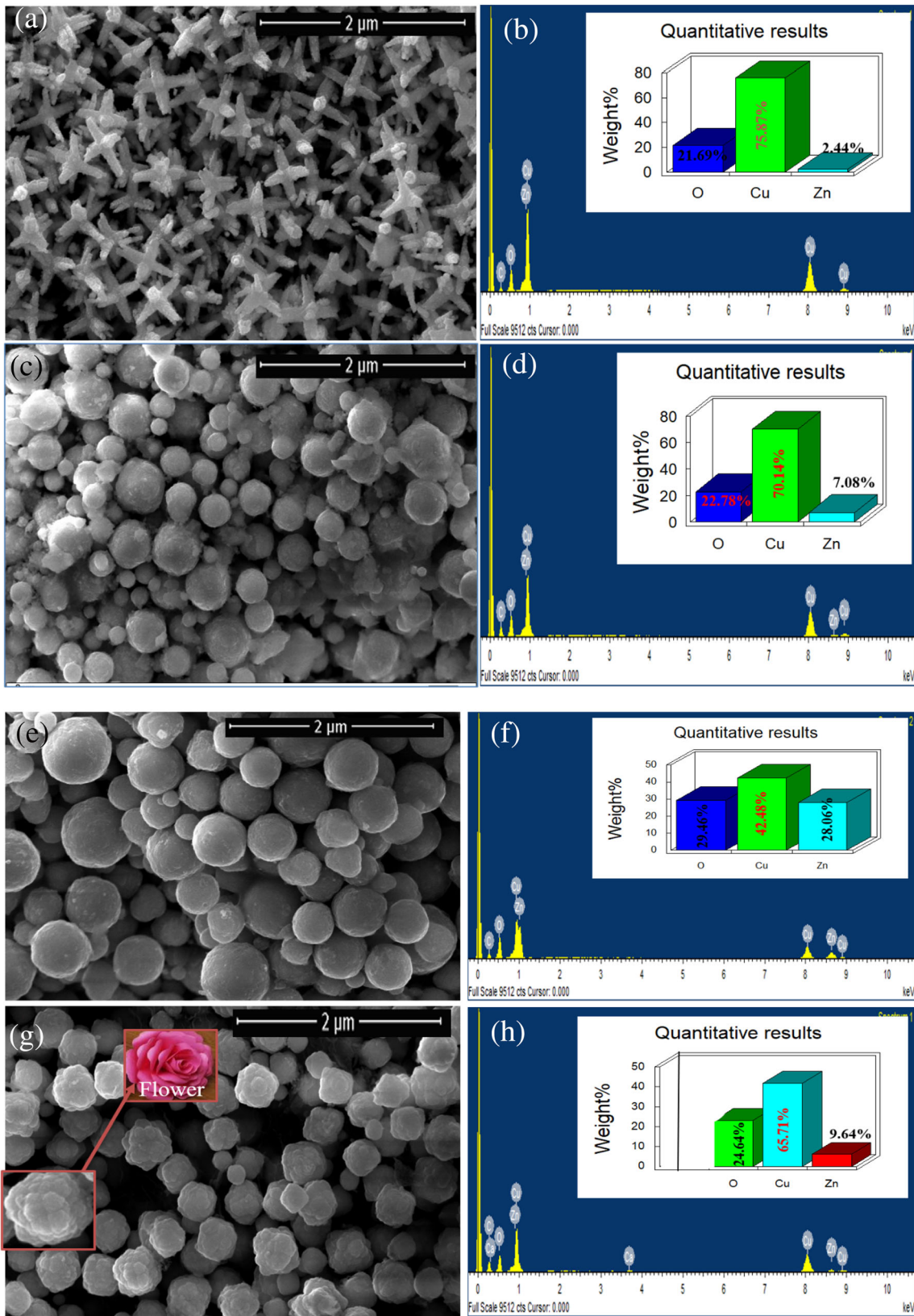


Fig. 3 SEM images and their corresponding EDX spectra of a, b 90:10, c, d 80:20, e, f 70:30, and g, h 60:40 CuO/Cu₂O-ZnO nanocomposites

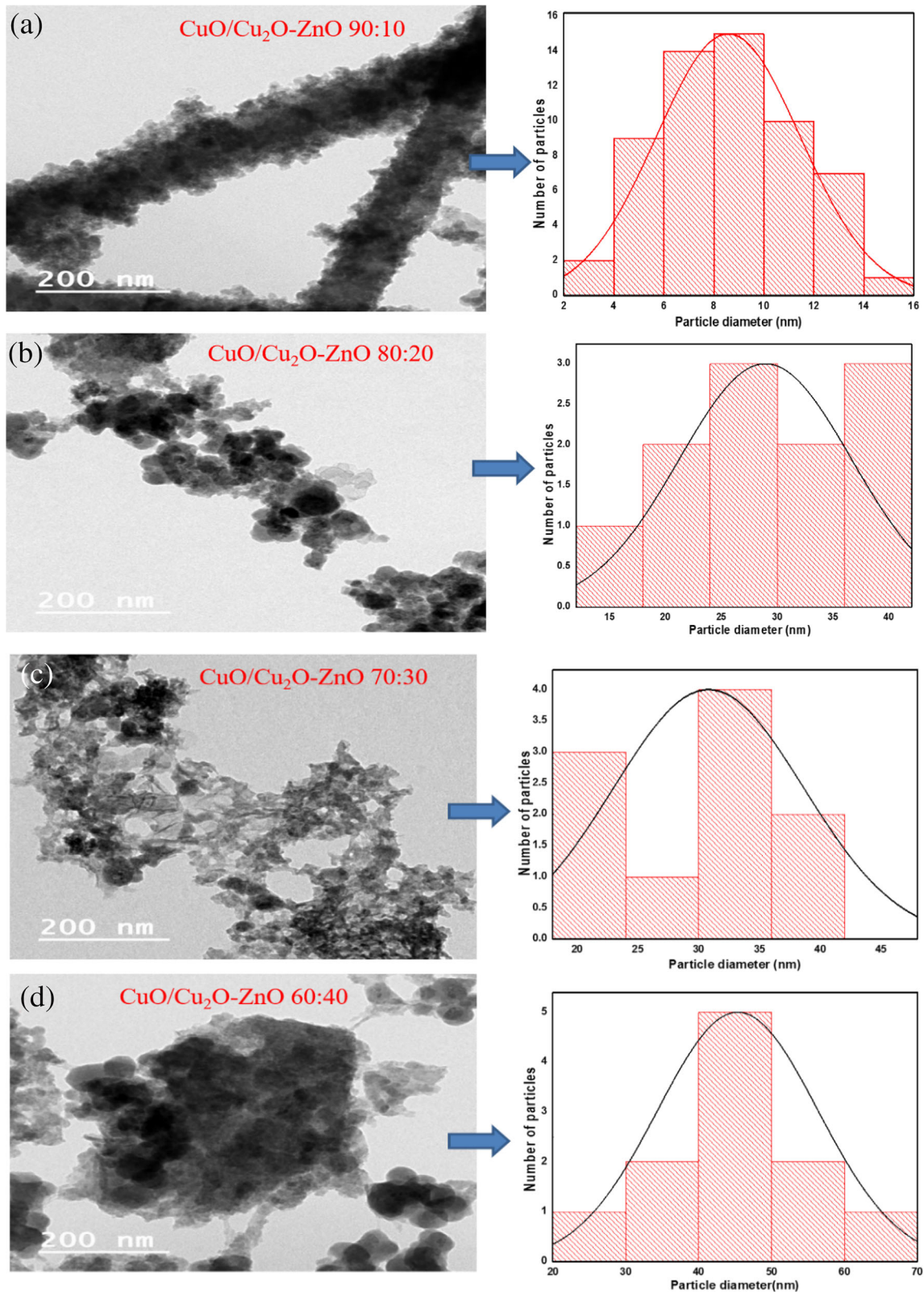


Fig. 4 TEM images of a 90:10, b 80:20, c 70:30 and d 60:40 of CuO/Cu₂O-ZnO nanocomposites, and their corresponding particles size distribution

combination with the green method is a simple, cost-effective, and convenient method for the synthesis of nanomaterials [20, 21]. The researchers have been synthesized $\text{Cu}_2\text{O}/\text{CuO}-\text{ZnO}$ NCs in *Alchornea cordifolia* leaf extract by using hydrothermal method [22] and ZnO/CuO NCs in *Mentha longifolia* leaf extract through microwave assisted method for anticancer and antibacterial activities [23].

Ipomoea carnea is a plant species belonging to the Genus *Ipomoea*, commonly called as the pink morning glory. The various parts of the plant are being widely used for their antibacterial, antifungal, antioxidant, anticancer, and anti-inflammatory properties. *Ipomoea carnea* possesses polyphenols and

alkaloids that can be used as reducing and stabilizing agents during the synthesis of nanoparticles [24]. The antimicrobial properties of nanoparticles synthesized by using *Ipomoea carnea* are well established, and several researchers have proposed a mechanism of inhibition [25, 26].

In this study, for the first time, the *Ipomoea carnea* leaf extract has been explored to synthesize $\text{CuO}/\text{Cu}_2\text{O}-\text{ZnO}$ NCs at different ratios of precursors, $[\text{Cu}(\text{CH}_3\text{COO})_2 \cdot \text{H}_2\text{O}]$ and $[\text{Zn}(\text{CH}_3\text{COO})_2 \cdot 2\text{H}_2\text{O}]$ under microwave-irradiation. Furthermore, the microwave-assisted green method will prove to be an innovative technique to explore the antioxidant,

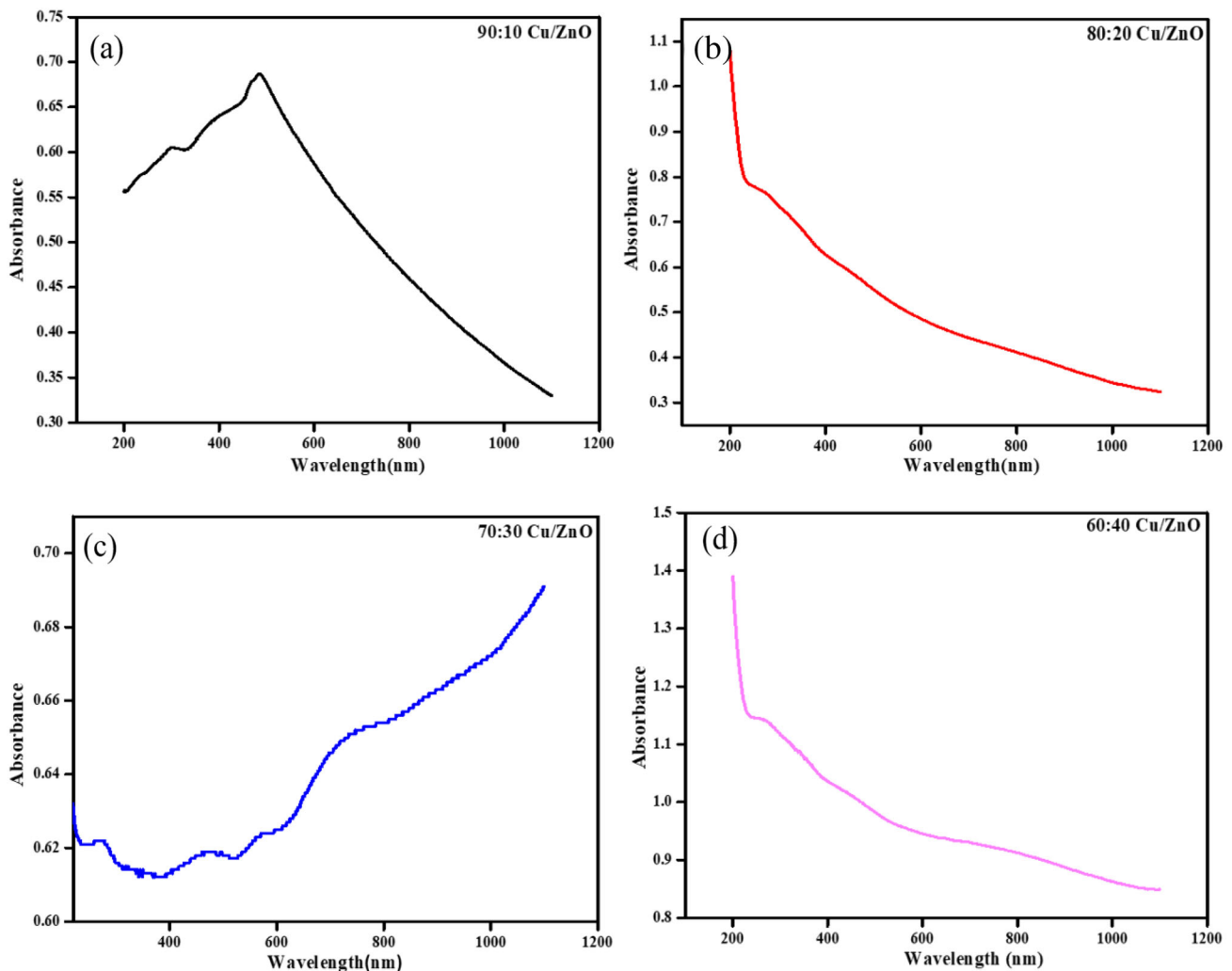


Fig. 5 UV-Visible spectra of **a** 90:10, **b** 80:20, **c** 70:30 and **d** 60:40 of $\text{CuO}/\text{Cu}_2\text{O}-\text{ZnO}$ nanocomposites

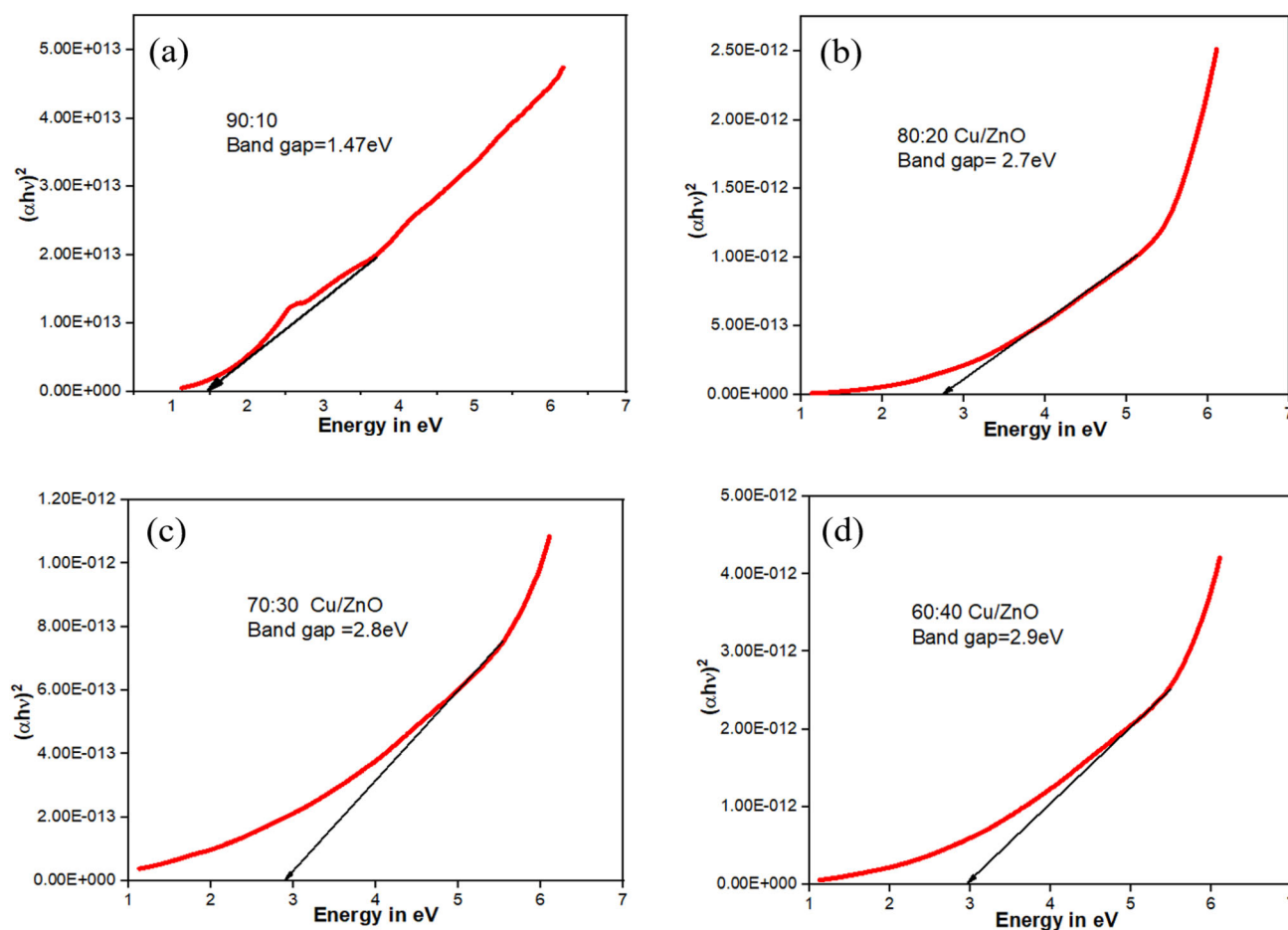


Fig. 6 The band gap values (Tauc plots) of **a** 90:10, **b** 80:20, **c** 70:30 and **d** 60:40 CuO/Cu₂O-ZnO nanocomposites

Table 2 Energy band gaps of various synthesized CuO/Cu₂O-ZnO nanocomposites

CuO/Cu ₂ O-ZnO	E _g (eV)
90:10	1.47
80:20	2.7
70:30	2.8
60:40	2.9

photocatalytic, and antibacterial activities of the as-synthesized CuO/Cu₂O-ZnO NCs.

2 Experimental section

2.1 Materials

All chemicals used in the experiments, including Cu(CH₃COO)₂·H₂O, Zn(CH₃COO)₂·2H₂O, NaOH, C₂H₅OH, methyl orange (MO), methylene blue (MB), Agar-agar Type I, Mueller Hinton broth, Nutrient agar, H₂O₂, 2,2-diphenyl-2-picryl hydrazyl hydrate

(DPPH), and ascorbic acid, were purchased from Merck Pvt. Ltd. and used without additional purification. Pathogens, namely *Staphylococcus aureus* (MTCC 737), *Bacillus subtilis* (MTCC 441), and *Escherichia coli* (MTCC 739), were procured from CSIR-IMTECH in Chandigarh, India. The green leaves of the *Ipomoea carnea* plant were collected from surroundings of the University Campus at Hamirpur, Himachal Pradesh.

2.2 Methods

2.2.1 Preparation of the leaf extract

To prepare the plant leaf extract, the green leaves of *Ipomoea carnea* were thoroughly washed with tap water and then rinsed with distilled water 2–3 times. The leaves were then dried in a hot air oven at 60 °C and crushed into a fine powder. 5 gm of the powder was dissolved in 100 ml of distilled water and refluxed at 80 °C for approximately 45 min. The

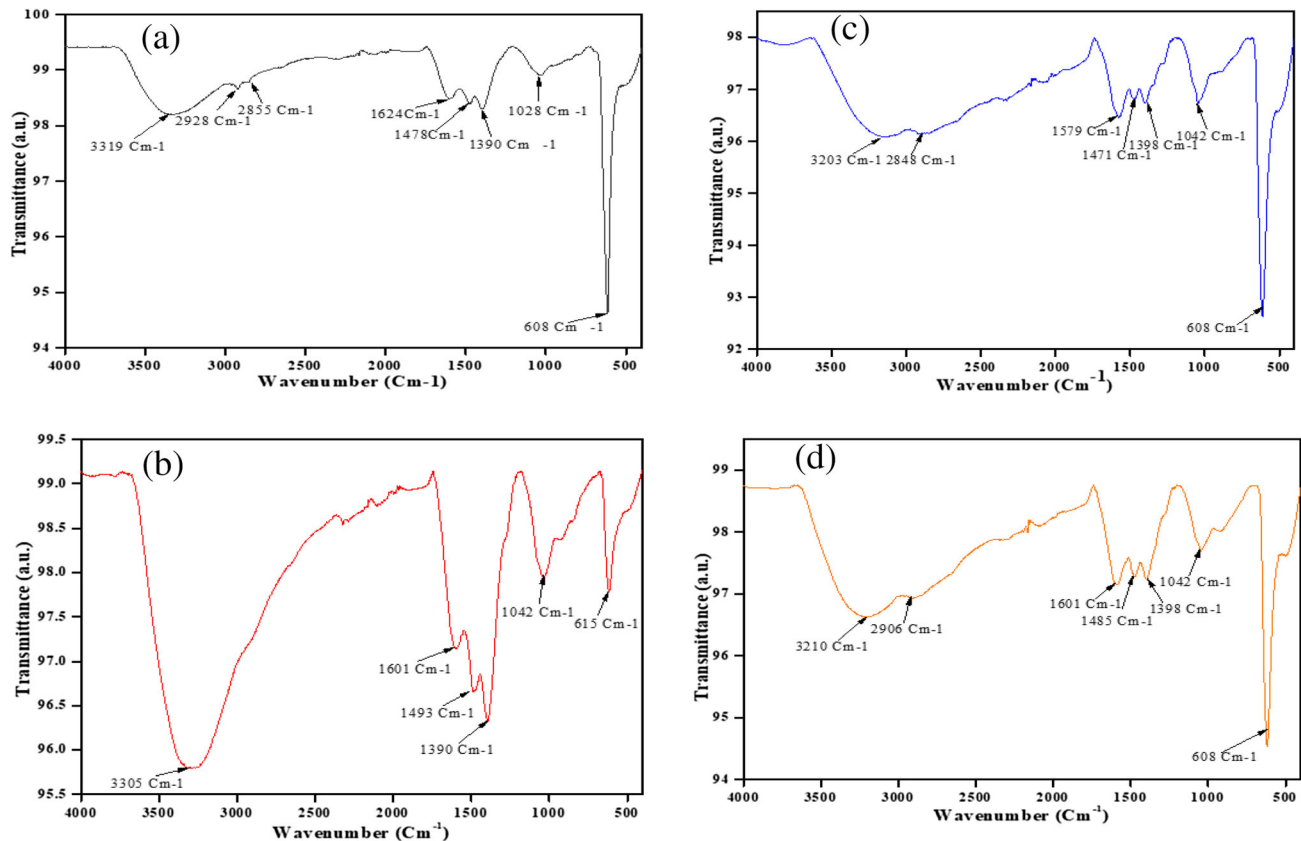


Fig. 7 FTIR spectra of **a** 90:10, **b** 80:20, **c** 70:30, and **d** 60:40 CuO/Cu₂O-ZnO nanocomposites

Table 3 Absorption bands and corresponding functional groups for various CuO/Cu₂O-ZnO nanocomposites

Vibration	$\bar{\nu}$ (cm ⁻¹)			
	90:10	80:20	70:30	60:40
OH	3319	3305	3203	3210
C-H stretch	2928, 2855	—	2848	2906
C=O	1624	—	—	1601
CH ₃ bend	1478	1493, 1390	1471, 1398	1485, 1398
C-O stretch	1028	1042	1042	1042
Cu-O/ZnO	608	615	608	608

resulting plant leaf extract was filtered using Whatman filter paper No. 1 and stored at 4 °C for use in the synthesis of CuO/Cu₂O-ZnO NCs [27].

2.2.2 Synthesis of the nanocomposites

A microwave oven operating at 2.45 GHz and 700 W power was employed to synthesize CuO/Cu₂O-ZnO nanocomposites using *Ipomoea carnea* leaf extract. Copper acetate and zinc acetate were mixed in a

10 mM solution, respectively, and then mixed in ratios of 90:10, 80:20, 70:30, and 60:40%. To each solution, 20 ml of the prepared leaf extract was added dropwise. The pH of the solution was adjusted to 12 by slowly adding an aqueous solution of 1 M NaOH. The solution was then irradiated in the microwave oven for 20 min, resulting in a color change from green to dirty green and ultimately dark brown, indicating the formation of CuO/Cu₂O-ZnO NCs. The resulting precipitates were washed several times with DW and ethanol, then dried in an oven at 70–80 °C for 24 h. Scheme 1 illustrates the synthesis of CuO/Cu₂O-ZnO NCs.

2.2.3 Antioxidant activity

To evaluate the scavenging activity of the synthesized CuO/Cu₂O-ZnO NCs, a 2 ml methanolic solution was prepared, and the stable 2,2-diphenyl-2-picrylhydrazyl hydrate (DPPH 0.1 mM) was added at various concentrations (25, 50, 100, 200, 400, and 800 µg/ml) through serial dilution. After dilution, the samples were kept in the dark at room temperature

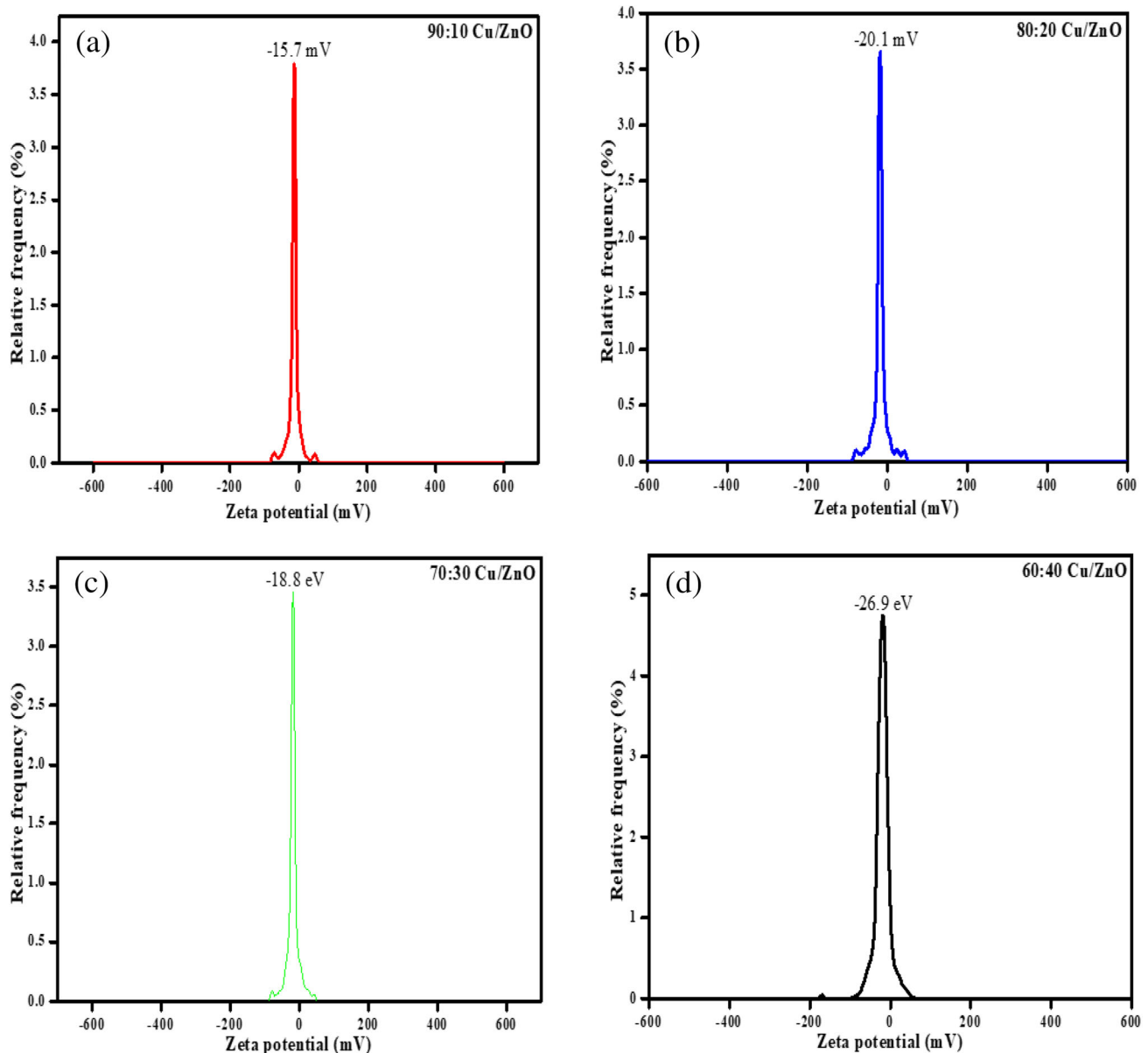


Fig. 8 Zeta potential measurement of prepared **a** 90:10, **b** 80:20, **c** 70:30, and **d** 60:40 CuO/Cu₂O-ZnO nanocomposites

for approximately 15–20 min. UV-Visible spectrophotometry was used to measure the change in color from deep violet to light yellow at 517 nm, indicating DPPH scavenging by the NCs [28].

2.2.4 Photocatalytic activity

A high-pressure mercury vapor lamp (125 W) was used as a UV light source. The lamp was placed vertically at a height of 6–7 cm above the reaction mixture. 100 ml of 10 ppm MB and MO solutions were treated with different amounts (5, 15, and 25 mg) of CuO/Cu₂O-ZnO NCs. The progress of the

reaction was observed by measuring the decrease in absorbance of λ_{\max} values for both dyes using UV-Visible spectrophotometry at 5-min intervals [29]. The structure of MO and MB dyes are shown in Fig. 1.

2.2.5 Antibacterial activity

The antibacterial activities of the synthesized samples were evaluated using the well diffusion method [30, 31] against Gram-positive (*Bacillus subtilis*, *Staphylococcus aureus*) and Gram-negative (*Escherichia coli*) bacteria. Furthermore, using the broth micro-

dilution method [32, 33], the minimum inhibitory concentration (MIC) and minimum bactericidal concentration (MBC) of the synthesized samples were determined. Each antibacterial experiment was performed in triplicate.

3 Results and discussion

3.1 Characterization

The X-ray diffraction (XRD) patterns in Fig. 2 of the prepared CuO/Cu₂O-ZnO nanocomposites show 2 θ peaks at 36.72°, 35.28°, 38.42°, 48.38°, 56.37°, 61.34°, 42.22°, and 73.52°, corresponding to (111), (002), (111), (202), (110), (113), (200), and (311) orientations of monoclinic and cubic phases for CuO/Cu₂O, respectively. These peaks are similar to the diffraction pattern of JCPDS 80-1268 and JCPDS file no. 05-0667 [3, 22]. The XRD peaks at 31.25°, 62.79°, 65.92°, 67.45°, and 69.39° represent (100), (103), (200), (112),

and (201) lattice indices attributed to the hexagonal wurtzite phase of ZnO (JCPDS file No-36-1451) [34]. The most intense peaks corresponding to Cu₂O-ZnO were found at (111)/(101), which indicates that the crystals are dominated by (111)/(101) facets of the

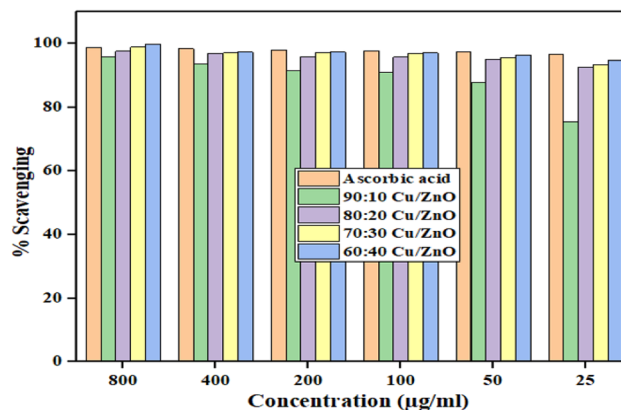


Fig. 10 The scavenging activity of different CuO/Cu₂O-ZnO nanocomposites in comparison with the standard ascorbic acid

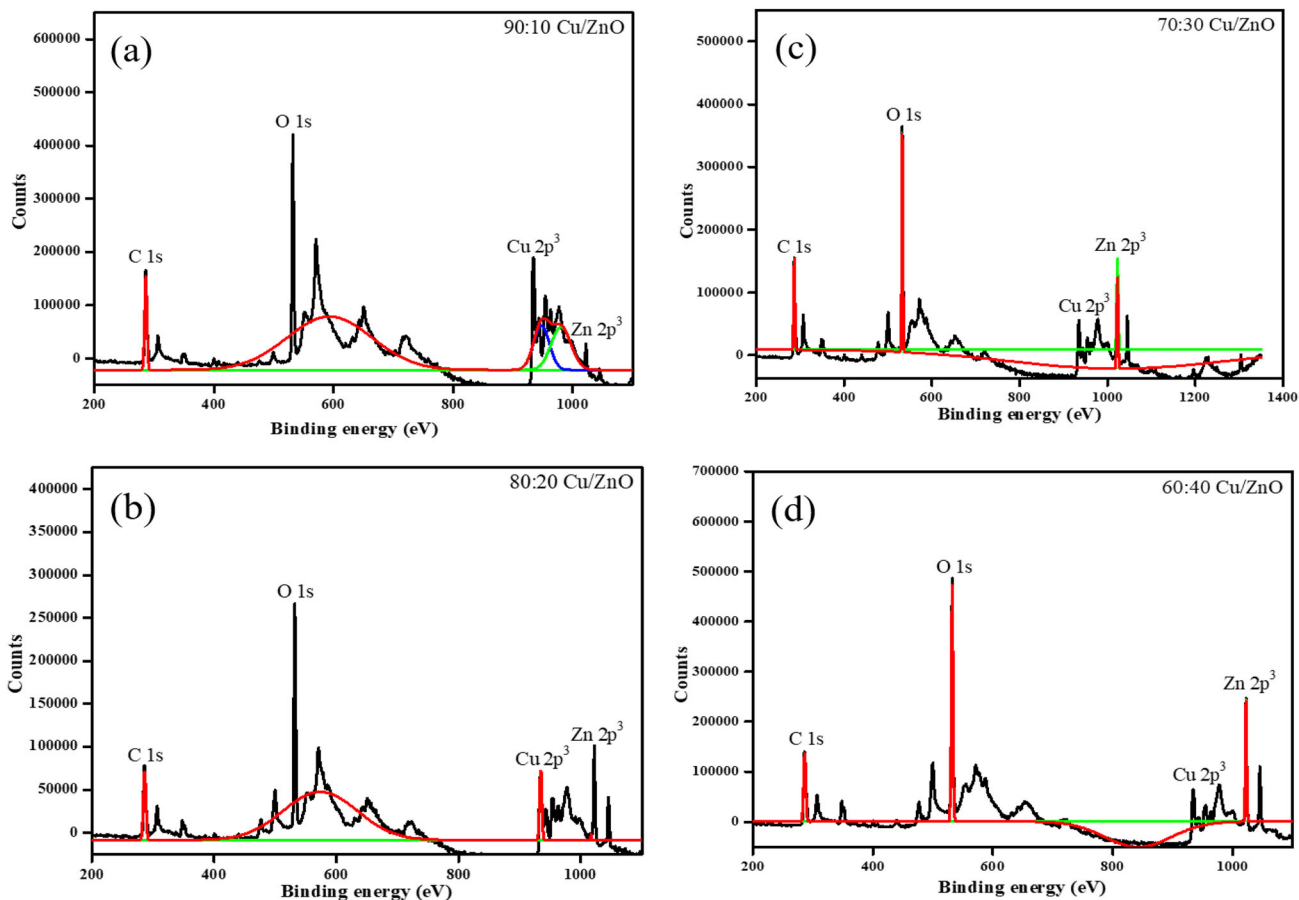


Fig. 9 XPS spectra of synthesized a 90:10, b 80:20, c 70:30, and d 60:40 CuO/Cu₂O-ZnO nanocomposites

Table 4 The percentage scavenging activity of different CuO/Cu₂O-ZnO nanocomposites at 800 µg/ml

Sample used CuO/Cu ₂ O-ZnO	Absorbance of pure control	Absorbance of control with sample	Free radical scavenging from DPPH assay (%)
90:10	0.438	0.011	97.48
80:20	0.438	0.006	98.63
70:30	0.438	0.005	98.86
60:40	0.438	0.001	99.77
Ascorbic acid	0.438	0.006	98.63

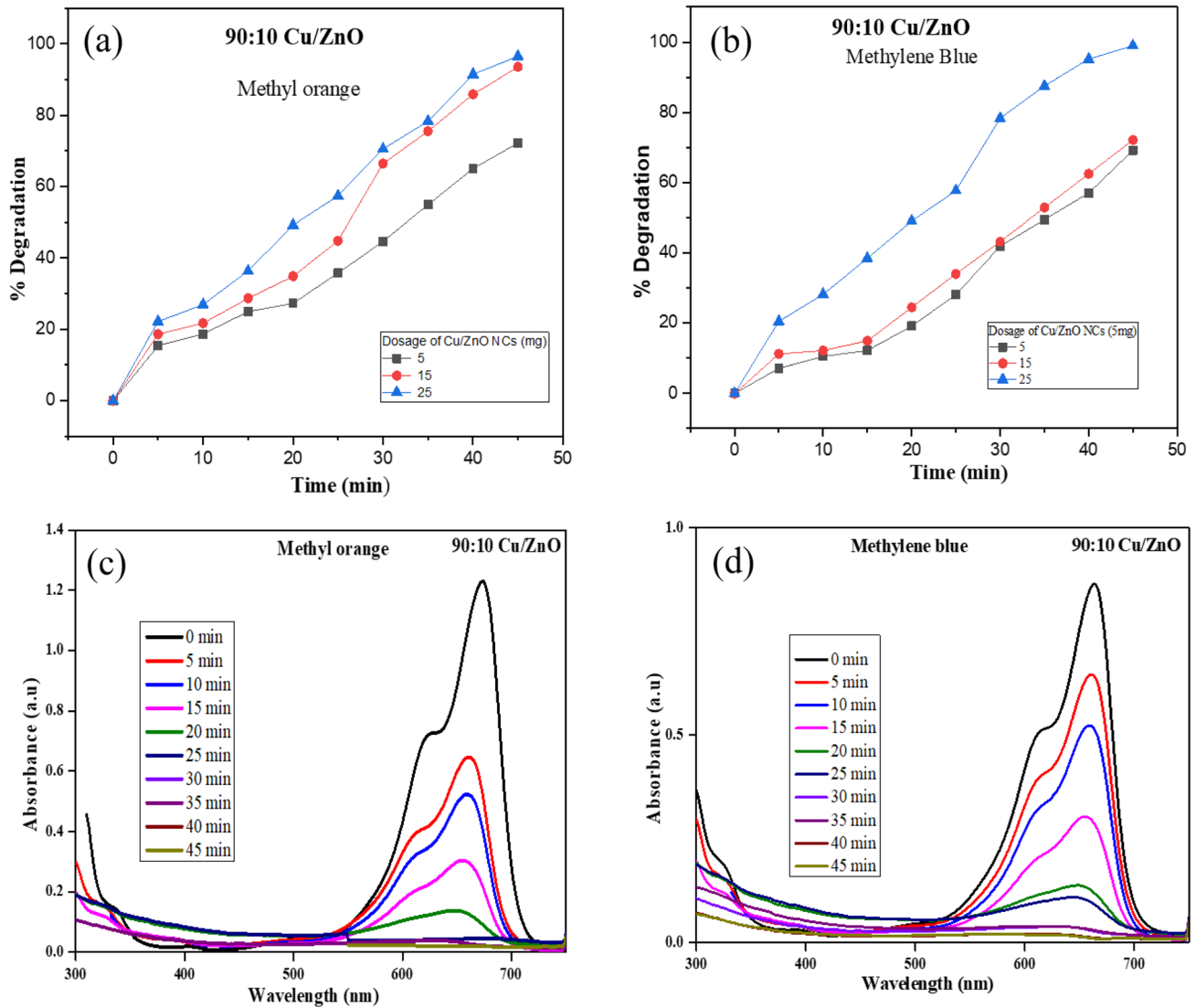


Fig. 11 Representative plots of degradation of a, c methyl orange and b, d methylene blue at various dosages of 90:10 CuO/Cu₂O-ZnO nanocomposites

CuO/Cu₂O-ZnO nanocomposites for all studied Cu:Zn ratios [35–37]. The crystallite size (*D*), dislocation density (δ), interplanar spacing (*d*), and microstrain (ϵ) of various CuO/Cu₂O-ZnO nanocomposites, as tabulated in Table 1, were calculated using the following equations [38, 39].

$$D = \frac{K\lambda}{\beta \cos \theta} \quad (1)$$

$$\delta = \frac{1}{D^2} \quad (2)$$

$$\epsilon = \frac{\beta \cos \theta}{4} \quad (3)$$

where *K* is Scherrers constant, which is 0.9, wavelength of the X-rays source is $\lambda = 0.15406$ nm, β is peak full width at half maximum (FWHM) of the intense peak and θ is Bragg's angle.

The formation of both CuO and Cu₂O phases may be occurring due to inadequate concentration of NaOH [22]. Additionally, previously reported studies show that oxidation temperatures below 300 °C also favor the formation of Cu₂O, while high oxidation temperatures lead to the formation of CuO [23].

SEM and EDX analysis were used to examine the morphology and elemental composition of the synthesized nanocomposites, as shown in Fig. 3. The micrographs show star, small sphere, large sphere, and flower-like structures of the different CuO/Cu₂O-ZnO nanocomposites with compositions of 90:10, 80:20, 70:30, and 60:40, respectively. The EDX spectra show a single composite peak for Cu-Zn and other separate peaks for C, O, Zn, and Cu. The different nanocomposites indicate the presence of all three elements with percentages in the order of Cu > Zn in all samples.

The size analysis of various synthesized NC samples was carried out using TEM spectroscopy. The TEM images, as shown in Fig. 4, depict the accumulated star/rod-like particles with an average size of 8–10 nm for 90:10 CuO/Cu₂O-ZnO NCs (Fig. 4a). In contrast, mixed spherical types, clusters of nanoblocks, and mixed nanospheres with an average size of 25–30, 30–35, and 40–50 nm for 80:20, 70:30, and 60:40 CuO/Cu₂O-ZnO NCs, respectively, can be seen in Fig. 4b–d. The uniform quantum size of CuO/Cu₂O-ZnO (90:10) is noteworthy and may be due to the higher concentration of the copper element. The subsequent increase in concentration of zinc in CuO/Cu₂O-ZnO NCs leads to an increase in particle size

from 8 to 50 nm (Fig. 4). The average particle size decreases with an increase in the Cu:Zn ratio from 60:40 to 90:10. Mohammadi-Aloucheh et al. [40] reported similar results, particularly with regards to the decreased average size of NCs.

The UV-Visible spectra of various samples are illustrated in Fig. 5. The UV absorbance bands appear at 485, 234, 491, and 243 nm for the various synthesized CuO/Cu₂O-ZnO NCs, as shown in Fig. 5. The intensities of absorption peaks and bandgap of various samples depend on a variety of factors such as the method of synthesis, pH, particle size, temperature, topology, surface structure, impurities, oxygen vacancies, type of precursor, and concentrations used [37].

The evaluation of band gap values of synthesized CuO/Cu₂O-ZnO NCs is done by using following Tauc relation [22].

$$\alpha h\nu = A (h\nu - E_g)^{1/2} \quad (4)$$

where $h\nu$ is the photon energy, α is the optical absorption coefficient and *A* is the independent constant. Here *E_g* is the direct band gap.

The Tauc plots of the different samples are shown in Fig. 6, and the corresponding band gap (*E_g*) values are summarized in Table 2. The observed increase in *E_g* values may be attributed to the decrease in copper content in the Cu/ZnO NCs. These results suggest that the synthesized samples exhibit good optical properties. The calculated band gap values are smaller compared to pure ZnO nanoparticles, which is expected due to the small particle size and unique morphology of the CuO/Cu₂O-ZnO NCs [6–8].

The synthesized CuO/Cu₂O-ZnO NCs were characterized for various functional groups using FTIR spectroscopy, as shown in Fig. 7. The wave numbers corresponding to the functional groups present in the samples are tabulated in Table 3. The peaks obtained at around 3319, 3305, 3203, and 3210 cm⁻¹ indicate the presence of O–H stretching modes of vibration from bio-components such as phenolic compounds. There are four peaks at around 2928, 2906, 2855, and 2848 cm⁻¹ due to C–H stretching vibrations, either from CH₂ or CH₃ groups from aliphatic compounds. The peaks at 1624 and 1601 cm⁻¹ are attributed to the carbonyl group, most likely due to aldehydes, ketones or esters. The peaks at 1471, 1485, 1498, 1478, 1390, 1398, and 1028, 1042 cm⁻¹ are related, respectively, to the C–C bending and C–O stretching

Table 5 Percentage of photo degradation of methyl orange (MO) and methylene blue (MB) dyes at different dosage of CuO/Cu₂O–ZnO nanocomposites

CuO/Cu ₂ O–ZnO	NCs dosage (mg)	Time (min)	Degradation of dye (%)	
			MO	MB
90:10	5	45	72.16	69.21
	15	45	93.47	72.12
	25	45	96.45	98.96
80:20	5	45	67.25	58.59
	15	45	74.05	66.44
	25	45	78.62	88.30
70:30	5	45	55.99	48.17
	15	45	62.28	55.39
	25	45	68.81	81.52
60:40	5	45	48.34	31.75
	15	45	53.51	52.64
	25	45	59.65	76.45

vibrations. The bands around 608 and 615 cm⁻¹ are due to the M–O bond stretching [41, 42].

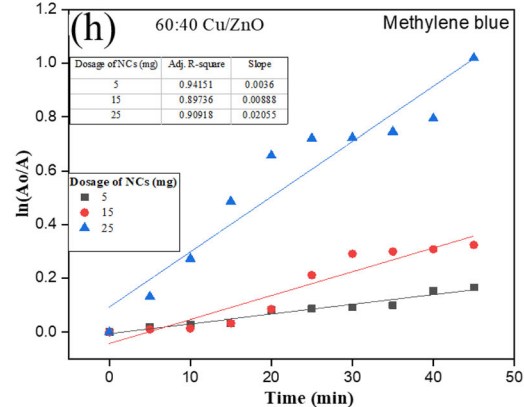
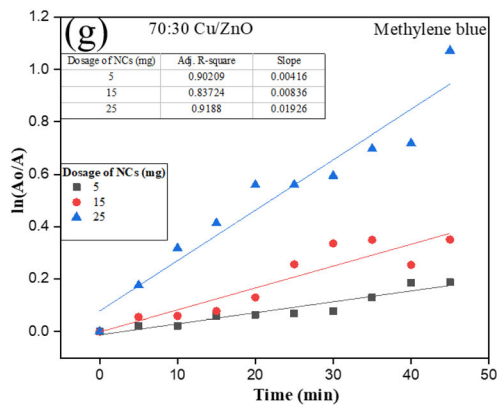
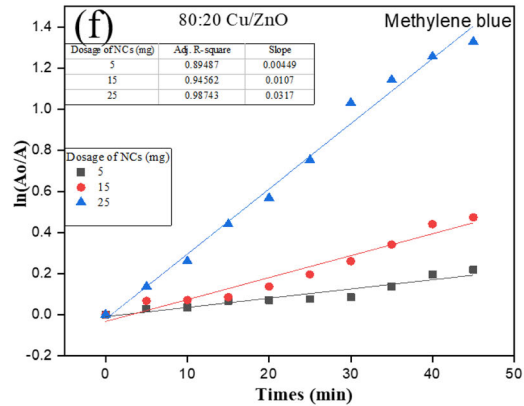
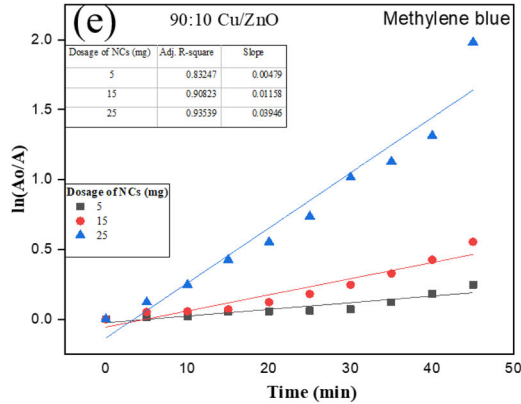
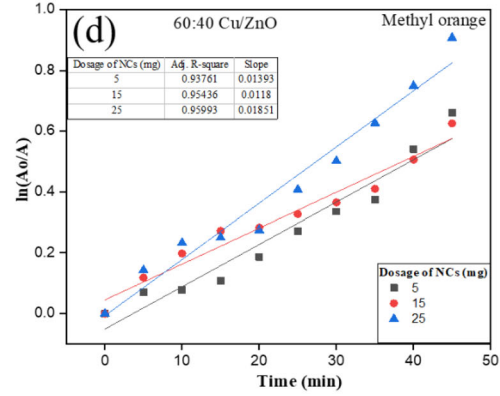
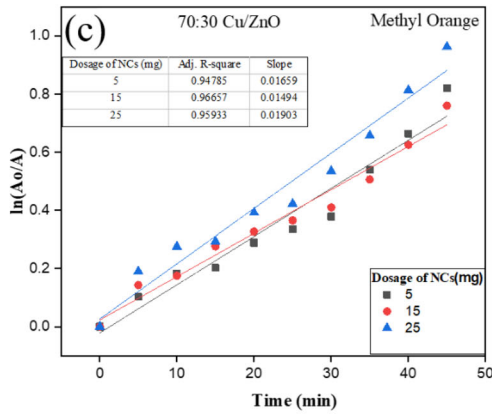
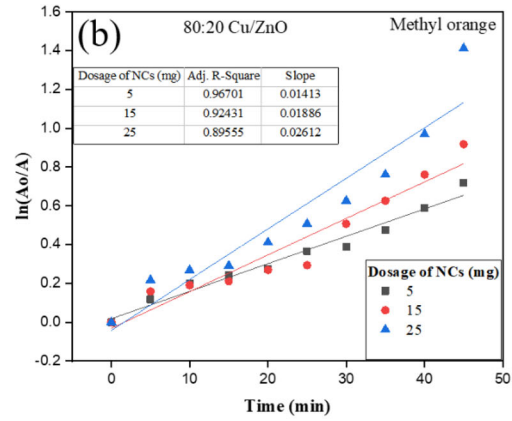
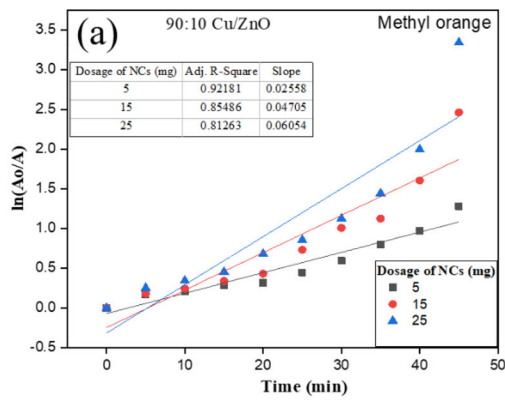
Moreover, the zeta potential of the biosynthesized Cu/ZnO NCs indicated a negative surface charge, ranging from –15.7 to –26.9 mV, as shown in Fig. 8, which may be due to the stabilization of the biomolecular components of *Ipomoea carnea* leaf extract on the surface of the samples after the reduction process. The negative surface charge of the prepared Cu/ZnO NCs further leads to the production of strong electrostatic repulsion forces among the particles, thereby stabilizing the nanoparticles by reducing their accumulation. The negative surface charge of nanoparticles synthesized using leaf extracts is well described in the literature [43, 44].

The purity of the synthesized Cu/ZnO nanocomposites was further characterized using X-ray photoelectron spectroscopy (XPS) technique. As shown in Fig. 9, the XPS spectra exhibit binding energy (BE) at ~ 933.87, 934.09, 934.31, and 933.89 eV corresponding to Cu 2p³ for 90:10, 80:20, 70:30, and 60:40 Cu/ZnO NCs, respectively. A highly intense peak at 532.01, 532.13, 532.3, and 532.12 eV corresponds to O-atom (O 1 s) bonded to Cu (II) and Zn (II) generating CuO and ZnO nanoparticles. The binding energy at ~ 285.9, 286.13, 286.02, and 285.99 for a C 1 s electron, and the peaks at ~ 1022.12, 1022.21, 1022.5, and 1022.2 eV correspond to Zn 2p³ for all synthesized samples. These XPS findings are strongly supported by data already available [45–47], and confirmed that there are no impurities in the synthesized materials.

3.2 Antioxidant activity

1,1-diphenyl-2-picrylhydrazyl (DPPH) is a stable nitrogen-centered free radical that is commonly used to test the radical scavenging activities of samples. The antioxidant activity of composite nanomaterials is one of their most important applications [48, 49], as it plays a crucial role in all living systems. In the present study, the microwave-synthesized CuO/Cu₂O–ZnO NCs exhibit excellent antioxidant activity at different concentrations, as shown in Fig. 10. This may be attributed to the presence of capping agents from the leaf extract, which are reported to play a significant role in free radical scavenging activities. The scavenging activity of various CuO/Cu₂O–ZnO NCs samples was compared with ascorbic acid used as a standard, as shown in Fig. 10.

The percentage scavenging activity was calculated using Eq. (5) and summarized in Table 4. It can be observed from Table 4 that the 60:40 CuO/Cu₂O–ZnO NCs show more scavenging activity than other synthesized NCs with 800 µg/ml DPPH solution. Notably, approximately 99.77% scavenging takes place (Table 4), while ascorbic acid reported approximately 98.66% scavenging in 800 µg/ml DPPH solution as shown in Fig. 10. This result may be due to an increase in the Zn content in the NCs sample. Similar results have been reported by Siripireddy et al. [50] for the antioxidant activity of ZnO nanoparticles synthesized using *Eucalyptus globulus* plant extract. Parashant et al. [51] showed that biologically synthesized nanoparticles have higher antioxidant activities compared to chemically fabricated nanoparticles due to the presence of bioactive



◀ **Fig. 12** Plots of pseudo-first-order kinetics of MO and MB dyes degradation with time at 5, 15 and 25 mg of various CuO/Cu₂O-ZnO nanocomposites (a–h)

phytochemicals such as flavonoids, alkaloids, and phenolic compounds from the plant leaf extract.

$$\begin{aligned} & \% \text{ scavenging activity} \\ & = \frac{\text{Absorbance of pure control} - \text{Absorbance of control with sample}}{\text{Absorbance of pure control}} \\ & \times 100 \end{aligned} \tag{5}$$

3.3 Photocatalytic activity

The photocatalytic activity of CuO/Cu₂O-ZnO NCs synthesized through microwave-assisted methods was studied by subjecting them to UV-light (125 W) in the presence of 10 μl H₂O₂ for the degradation of industrial pollutants methylene blue (MB) and methyl orange (MO) [52, 53]. UV-Visible spectra were recorded from 400 to 800 nm at intervals of 5 min up to 45 min, and the characteristic peaks of MB and MO were identified at 668 nm and 464 nm, respectively [54], as shown in Fig. 11. Table 5

indicates that the synthesized samples exhibited high degradation efficiency, with 98.96 and 96.45% degradation of MB and MO, respectively, within 45 min. This rapid degradation can be attributed to the electron transfer process between the acceptor and donor due to the transitional redox potential, with the CuO/Cu₂O-ZnO NCs acting as excellent redox catalysts due to their electron releasing effect [55]. Additionally, the size of the NCs played a crucial role in the catalytic degradation, as observed in Table 5. The 90:10 CuO/Cu₂O-ZnO NCs with the smallest size among all samples provided a larger surface area for the adsorption of reactants, leading to the highest degradation of MB (98.96%) and MO (96.45%). The percentage dye degradation was evaluated as described in [56, 57].

$$\% \text{ Degradation} = \frac{A_o - A_t}{A_o} \times 100 \tag{6}$$

where A_o and A_t are the absorption of pure solution and reaction mixture at time ‘t’

Also, the kinetics of the degradation reaction (Fig. 12) determined by using Eq. (7) [3].

$$\ln\left(\frac{A_o}{A}\right) = \ln\left(\frac{C_o}{C_t}\right) = -kt \tag{7}$$

Fig. 13 Zones of inhibition of (i) 90:10, (ii) 80:20, (iii) 70:30, and (iv) 60:40 CuO/Cu₂O-ZnO nanocomposites against (a–d) *B. subtilis*, (e–h) *S. aureus* and (i–l) *E. coli*, respectively

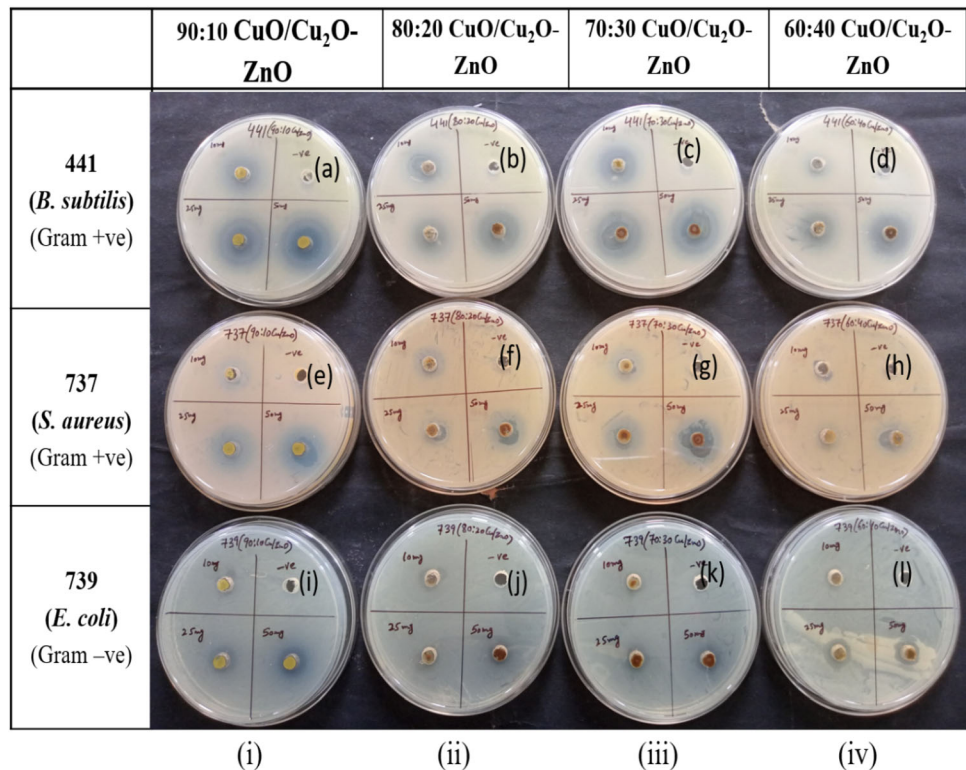


Table 6 The zones of inhibition with different dosages of various synthesized CuO/Cu₂O-ZnO nanocomposites for three bacteria

Bacteria	CuO/Cu ₂ O-ZnO	NCs dosage (mg.ml ⁻¹)	Zone of inhibition (mm)	
<i>B. subtilis</i>	90:10	10	26.83 ± 0.44 ^a	
		25	33.86 ± 0.46	
		50	36.83 ± 0.44	
	80:20	10	21.66 ± 0.88	
		25	24.83 ± 0.44	
		50	31 ± 0.57	
	70:30	10	26.33 ± 0.88	
		25	30.33 ± 0.33	
		50	32.33 ± 0.33	
	60:40	10	11.33 ± 0.66	
		25	22 ± 0.57	
		50	27.16 ± 0.72	
	<i>S. aureus</i>	90:10	10	17.5 ± 0.76
			25	23 ± 1.15
			50	25.66 ± 0.88
80:20		10	14.33 ± 1.20	
		25	16.66 ± 1.45	
		50	18.33 ± 0.88	
70:30		10	17.33 ± 0.88	
		25	19.33 ± 2.33	
		50	24.66 ± 0.33	
60:40		10	10 ± 1.73	
		25	14 ± 0.57	
		50	17.66 ± 0.88	
<i>E. coli</i>		90:10	10	11.33 ± 0.88
			25	16 ± 0.57
			50	17.33 ± 0.33
	80:20	10	12 ± 0.57	
		25	13 ± 0.57	
		50	12.5 ± 0.76	
	70:30	10	10.33 ± 0.88	
		25	12.83 ± 0.44	
		50	15.33 ± 0.33	
	60:40	10	10 ± 0.57	
		25	13.66 ± 0.88	
		50	14.33 ± 0.66	

^aStandard error in measurement of zone of inhibition (mm)

where C_0 = initial concentration of dye, C_t = concentration of dye at time 't', k = pseudo-first-order rate constant.

The pseudo-first-order reaction kinetics can be clearly observed in Fig. 12, which depicts a linear relationship between $\ln A_0/A$ and time 't' [37]. The pseudo-first-order rate constant k was calculated for CuO/Cu₂O-ZnO NCs synthesized at different Cu:Zn ratios (90:10, 80:20, 70:30, and 60:40) with 5, 15, and 25 mg catalytic load, and the results showed that the

minimum and maximum values of k were 0.0118 min⁻¹ and 0.0605 min⁻¹ for MO, and 0.0036 min⁻¹ and 0.0394 min⁻¹ for MB [29]. Additionally, the correlation constants R^2 of the fitted lines ranged from 0.8126 to 0.9599 for MO and from 0.9091 to 0.9353 for MB at 25 mg catalytic load.

3.4 Anti-bacterial activity

The antibacterial activity of CuO/Cu₂O-ZnO nanocomposites synthesized at different

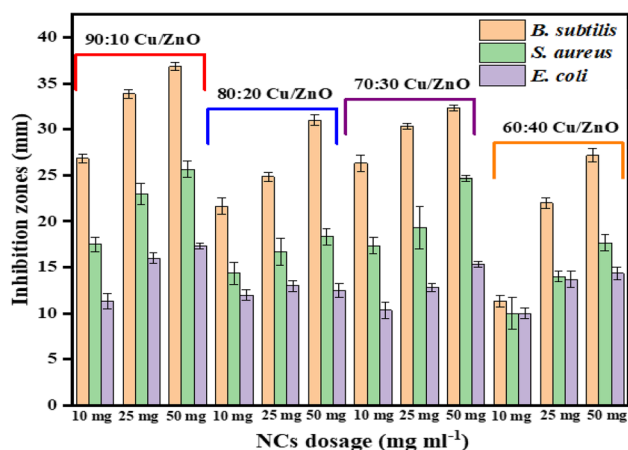


Fig. 14 Zone of inhibition of *B. subtilis*, *S. aureus* and *E. coli* with 10, 25 and 50 mg dosages of 90:10, 80:20, 70:30 and 60:40 CuO/Cu₂O-ZnO nanocomposites

Table 7 MIC and MBC values of CuO/Cu₂O-ZnO nanocomposites and ciprofloxacin for various studied bacteria

Bacteria	CuO/Cu ₂ O-ZnO	MIC (µg ml ⁻¹)	MBC (µg ml ⁻¹)
<i>B. subtilis</i>	90:10	390.625	1562.5
	80:20	3125	6250
	70:30	1562.5	3125
	60:40	6250	12,500
	Ciprofloxacin	< 1	< 0.5
<i>S. aureus</i>	90:10	1562.5	6250
	80:20	3125	12,500
	70:30	3125	6250
	60:40	3125	12,500
	Ciprofloxacin	16.65	1
<i>E. coli</i>	90:10	1562.5	3125
	80:20	3125	12,500
	70:30	1562.5	6250
	60:40	3125	12,500
	Ciprofloxacin	< 1	0.5

concentrations was investigated using the well diffusion method against three bacterial strains: *B. subtilis*, *S. aureus*, and *E. coli* [30, 31]. The scale was used to measure the zone of inhibition (ZOI) (Fig. 13). However, as shown in Table 6 and Fig. 14, *B. subtilis* showed the highest ZOI for all the synthesized CuO/Cu₂O-ZnO NCs, followed by *S. aureus* and *E. coli*, due to the differences in their gram staining characteristics. Among all the samples prepared, the star/rod-shaped (90:10 CuO/Cu₂O-ZnO) NCs were found to be the most effective. The maximum ZOI of 36.83 ± 0.44 was observed for *B. subtilis*, followed by

S. aureus and *E. coli* (Table 6). The measured minimum inhibitory concentration (MIC) and minimum bactericidal concentration (MBC) values (Table 7) ranged between 390.625–6250 µg.ml⁻¹ and 1562–12,500 µg.ml⁻¹, respectively. The synthesized CuO/Cu₂O-ZnO NCs exhibited greater efficiency compared to chemically synthesized pure CuO and ZnO nanoparticles [31, 32, 58, 59]. The antibacterial action of the nanocomposites can be attributed to the generation of reactive oxygen species (ROS), dispersion into the bacterial cell wall, and release of ions [60, 61]. The small size of CuO/Cu₂O-ZnO NCs makes it easy for them to penetrate the bacterial cell wall, causing the leakage of cell material and ultimately resulting in cell death, as illustrated in Fig. 15 [62–64]. A comparison of the multifunctionality performance of the synthesized CuO/Cu₂O-ZnO nanocomposites with previously reported studies on green synthesis has also been tabulated in Table 8.

4 Conclusions

The synthesized biogenic samples have been confirmed to have well-crystallized monoclinic, cubic, and hexagonal structures for CuO/Cu₂O and ZnO phases. TEM micrographs revealed the formation of various synthesized NCs such as stars (8–10 nm), mixed spherical (25–30 nm), clusters of nano-blocks (30–35 nm), and mixed nanospheres (40–50 nm). The energy band gap values ranged from 1.47 to 2.9 eV, and the stability of samples was measured through zeta potential values ranging between – 15.7 mV to – 26.9 mV. The purity and different bonding patterns of the synthesized materials were determined by XPS analysis. The synthesized NCs showed high antioxidant activity, with 99.77% scavenging of DPPH free radicals in 800 µg/ml for 60:40 CuO/Cu₂O-ZnO NCs. Moreover, the photocatalytic activity of 90:10 CuO/Cu₂O-ZnO NCs demonstrated about 98.96 and 96.45% degradation of 100 ml of 10 ppm of MB and MO dye solutions, respectively, in 45 min. The antibacterial activity revealed the high potential of CuO/Cu₂O-ZnO NCs against Gram +ve (*B. subtilis* and *S. aureus*) as compared to Gram –ve (*E. coli*) bacteria, with reported MIC and MBC values between 390.625–6250 and 1562–12,500 µg.ml⁻¹, respectively. The star-shaped (90:10 CuO/Cu₂O-ZnO) NCs demonstrated strong antibacterial and photocatalytic activities due to their small size, while

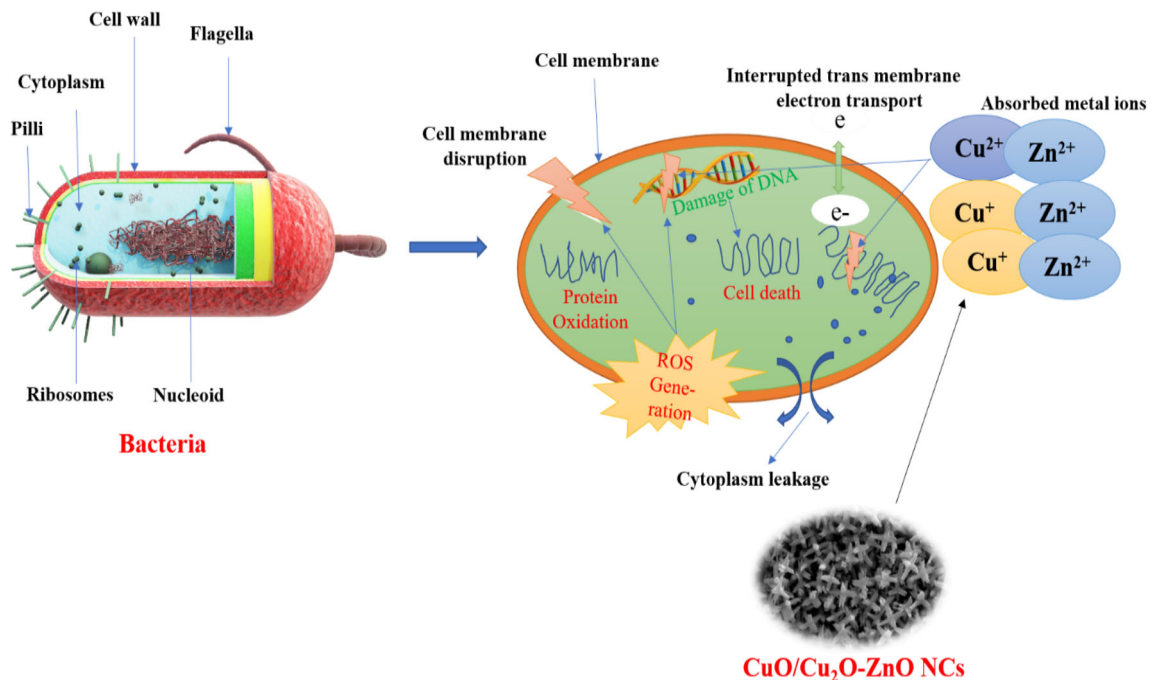


Fig. 15 Mechanism for the antibacterial action of synthesized CuO/Cu₂O-ZnO nanocomposites

Table 8 A comparison of the multi-functionality performance of the synthesized and previously reported nanocomposites on green method of synthesis

Type of nanomaterials synthesized	Method of synthesis	Plant used	Applications	References
Cu ₂ O/CuO-ZnO	Hydrothermal technique	<i>Alchornea cordifolia</i>	Anticancer activity	[22]
ZnO/CuO	Microwave method	<i>Mentha longifolia</i>	Antibacterial activity	[23]
CuO/Cu ₂ O-ZnO	Microwave assisted green method	<i>Ipomoea carnea</i>	<i>In-vitro</i> antioxidant, photocatalytic and antibacterial activities	Present study

flower-shaped NCs were found to be more effective in antioxidant activity. The results suggest that the so-synthesized CuO/Cu₂O-ZnO NCs are more effective antibacterial and photocatalytic agents compared to chemically synthesized NCs previously reported in the literature.

Acknowledgements

The authors are grateful to Department of Chemistry and Centre for Nano-Science & Technology, Career Point University, Hamirpur (H.P.) for providing all the necessary facilities to conduct research work. The authors are also grateful to Indian Institute of Technology (IIT), Mandi (H.P.), Sophisticated Analytical

Instrumentation Facility, Panjab University and Sprint Testing Solutions, Mumbai for providing characterization facilities.

Author contribution

RK: investigation, writing-original draft preparation, formal analysis. SS; NT: draft preparation, editing. KK; NT: review, editing, supervision.

Data availability

All data generated or analyzed during this study are included only in the article.

Declarations

Conflict of interest The authors declare that they have no known competing financial interests.

References

1. K.K. Jaiswal, S. Dutta, C.B. Pohrmen, R. Verma, A. Kumar, A.P. Ramaswamy, Bio-waste chicken egg shell-derived calcium oxide for photocatalytic application in methylene blue dye degradation under natural sunlight irradiation. *Inorg. Nano-Met. Chem.* **51**, 995–1004 (2021). <https://doi.org/10.1080/24701556.2020.1813769>
2. W. Ahmad, K. KumarJaiswal, M. Amjad, *Euphorbia herita* leaf extract as a reducing agent in a facile green synthesis of iron oxide nanoparticles and antimicrobial activity evaluation. *Inorg. Nano-Met. Chem.* **51**, 1147–1154 (2020). <https://doi.org/10.1080/24701556.2020.1815062>
3. L. Xiong, H. Yu, C. Nie, Y. Xiao, Q. Zeng, G. Wang, B. Wang, H. Lv, Q. Li, S. Chen, Size-controlled synthesis of Cu₂O nanoparticles: size effect on antibacterial activity and application as a photocatalyst for highly efficient H₂O₂ evolution. *RSC Adv.* **7**, 51822–51830 (2017). <https://doi.org/10.1039/C7RA10605J>
4. C.B. Ong, L.Y. Ng, A.W. Mohammad, A review of ZnO nanoparticles as solar photocatalysts: synthesis, mechanisms and applications. *Renew. Sustain. Energy Rev.* **81**, 81536–81551 (2018). <https://doi.org/10.1016/j.rser.2017.08.020>
5. S. Ahmed, S.A. Chaudhry, S. Ikram, A review on biogenic synthesis of ZnO nanoparticles using plant extracts and microbes: a prospect towards green chemistry. *J. Photochem. Photobiol. B Biol.* **166**, 272–284 (2017). <https://doi.org/10.1080/24701556.2020.1815062>
6. A.B. Djurišić, X. Chen, Y.H. Leung, A.M.C. Ng, ZnO nanostructures: growth, properties and applications. *J. Mater. Chem.* **22**, 6526–6535 (2012). <https://doi.org/10.1039/C2JM16813H>
7. K. Qi, B. Cheng, J. Yu, W. Ho, Review on the improvement of the photocatalytic and antibacterial activities of ZnO. *J. Alloys Compd.* **727**, 792–820 (2017). <https://doi.org/10.1016/j.jallcom.2017.08.142>
8. R. Kumar, A. Umar, G. Kumar, H.S. Nalwa, Antimicrobial properties of ZnO nanomaterials: a review. *Ceram. Int.* **43**, 3940–3961 (2017). <https://doi.org/10.1016/j.ceramint.2016.12.062>
9. A.P. Ingle, N. Duran, M. Rai, Bioactivity, mechanism of action, and cytotoxicity of copper-based nanoparticles: a review. *Appl. Microbiol. Biotechnol.* **98**, 1001–1009 (2014). <https://doi.org/10.1016/j.rser.2017.08.020>
10. I. Hussain, N.B. Singh, A. Singh, H. Singh, S.C. Singh, Green synthesis of nanoparticles and its potential application. *Biotechnol. Lett.* **38**, 545–560 (2016). <https://doi.org/10.1007/s10529-015-2026-7>
11. J. Singh, G. Kaur, M. Rawat, A brief review on synthesis and characterization of copper oxide nanoparticles and its applications. *J. Bioelectron. Nanotechnol.* **1**, 1–9 (2016)
12. J.R. Peralta-Videa, Y. Huang, J.G. Parsons, L. Zhao, L. Lopez-Moreno, J.A. Hernandez-Viezas, J.L. Gardea-Torresdey, Plant-based green synthesis of metallic nanoparticles: scientific curiosity or a realistic alternative to chemical synthesis? *Nanotechnol. Environ. Eng.* **1**, 1–29 (2016). <https://doi.org/10.1007/s41204-016-0004-5>
13. A. Dey, Semiconductor metal oxide gas sensors: a review. *Mater. Sci. Eng. B.* **229**, 206–217 (2018). <https://doi.org/10.1016/j.mseb.2017.12.036>
14. S. Sultana, M.Z. Khan, K. Umar, M. Muneer, Electrical, thermal, photocatalytic and antibacterial studies of metallic oxide nanocomposite doped polyaniline. *J. Mater. Sci. Technol.* **29**, 795–800 (2013). <https://doi.org/10.1016/j.jmst.2013.06.001>
15. P.H.C. Camargo, K.G. Satyanarayana, F. Wypych, Nanocomposites: synthesis, structure, properties and new application opportunities. *Mater. Res.* **12**, 1–39 (2009). <https://doi.org/10.1590/S1516-14392009000100002>
16. Z. Mehmood, M. Ikram, M. Imran, A. Shahzadi, A. Haider, A. Ul-Hamid, W. Nabgan, J. Haider, S. Hayat, Z. *officinale*-doped silver/calcium oxide nanocomposites: catalytic activity and antimicrobial potential with molecular docking analysis. *Process Biochem.* **121**, 635–646 (2022). <https://doi.org/10.1016/j.procbio.2022.07.035>
17. R. Ahmad, K. Ansari, Enhanced sequestration of methylene blue and crystal violet dye onto green synthesis of pectin modified hybrid (Pect/AILP-Kal) nanocomposite. *Process Biochem.* **111**, 132–143 (2021). <https://doi.org/10.1016/j.procbio.2021.10.009>
18. R. Rajeswari, H.G. Prabu, Palladium-decorated reduced graphene oxide/zinc oxide nanocomposite for enhanced antimicrobial, antioxidant and cytotoxicity activities. *Process Biochem.* **93**, 36–47 (2020). <https://doi.org/10.1016/j.procbio.2020.03.010>
19. R. Song, Q. Shi, G.A.A. Abdrabboh, R. Wei, Characterization and antibacterial activity of the nanocomposite of half-fin anchovy (*Setipinna taty*) hydrolysates/zinc oxide nanoparticles. *Process Biochem.* **62**, 223–230 (2017). <https://doi.org/10.1016/j.procbio.2017.07.002>
20. S. Ahmed, M. Ahmad, B.L. Swami, S. Ikram, A review on plants extract mediated synthesis of silver nanoparticles for

- antimicrobial applications: a green expertise. *J. Adv. Res.* **7**, 17–28 (2016). <https://doi.org/10.1016/j.jare.2015.02.007>
21. U. Shanker, V. Jassal, M. Rani, B.S. Kaith, Towards green synthesis of nanoparticles: from bio-assisted sources to benign solvents. A review. *Inter. J. Environ. Anal. Chem.* **96**, 801–835 (2016). <https://doi.org/10.1080/03067319.2016.1209663>
 22. E.E. Elemike, D.C. Onwudiwe, M. Singh, Eco-friendly synthesis of copper oxide, zinc oxide and copper oxide-zinc oxide nanocomposites, and their anticancer applications. *J. Inorg. Organomet. Polym. Mater.* **30**, 400–409 (2020). <https://doi.org/10.1007/s10904-019-01198-w>
 23. R. Mohammadi-Aloucheh, A. Habibi-Yangjeh, A. Bayrami, S. Latifi-Navid, A. Asadi, Green synthesis of ZnO and ZnO/CuO nanocomposites in *Mentha longifolia* leaf extract: characterization and their application as anti-bacterial agents. *J. Mater. Sci. Mater. Electron.* **29**, 13596–13605 (2018). <https://doi.org/10.1007/s10854-018-9487-0>
 24. N. Chand, P.K. Rohatgi, Impact toughness of *Ipomoea carnea* particulate-polyester composite. *J. Mater. Sci. Lett.* **6**, 695–697 (1987). <https://doi.org/10.1007/BF01770929>
 25. I. Sondi, B. Salopek-Sondi, Silver nanoparticles as antimicrobial agent: a case study on *E. coli* as a model for Gram-negative bacteria. *J. Colloid Interface Sci.* **275**, 177–182 (2004). <https://doi.org/10.1016/j.jcis.2004.02.012>
 26. P. Jain, T. Pradeep, Potential of silver nanoparticle-coated polyurethane foam as an antibacterial water filter. *Biotechnol. Bioeng.* **90**, 59–63 (2005). <https://doi.org/10.1002/bit.20368>
 27. V.V. Gawade, N.L. Gavade, H.M. Shinde, S.B. Babar, A.N. Kadam, K.M. Garadkar, Green synthesis of ZnO nanoparticles by using *Calotropis procera* leaves for the photodegradation of methyl orange. *J. Mater. Sci. Mater. Electron.* **28**, 14033–14039 (2017). <https://doi.org/10.1007/s10854-017-7254-2>
 28. N.J. Sushma, B. Mahitha, K. Mallikarjuna, B. Raju, Bio-inspired ZnO nanoparticles from *Ocimum tenuiflorum* and their in vitro antioxidant activity. *Appl. Phys. A.* **122**, 1–10 (2016). <https://doi.org/10.1007/s00339-016-0069-9>
 29. S. Sharma, K. Kumar, N. Thakur, S. Chauhan, M.S. Chauhan, Eco-friendly *Ocimum tenuiflorum* green route synthesis of CuO nanoparticles: characterizations on photocatalytic and antibacterial activities. *J. Environ. Chem. Eng.* **9**, 105395 (2021). <https://doi.org/10.1016/j.jece.2021.105395>
 30. S. Sharma, K. Kumar, N. Thakur, S. Chauhan, M.S. Chauhan, The effect of shape and size of ZnO nanoparticles on their antimicrobial and photocatalytic activities: a green approach. *Bull. Mater. Sci. Lett.* **43**, 1–10 (2020). <https://doi.org/10.1007/s12034-019-1986-y>
 31. N. Thakur, K. Kumar, Effect of (Ag, Co) co-doping on the structural and antibacterial efficiency of CuO nanoparticles: a rapid microwave assisted method. *J. Environ. Chem. Eng.* **8**, 104011 (2020). <https://doi.org/10.1016/j.jece.2020.104011>
 32. N. Thakur, K. Kumar, A. Kumar, Effect of (Ag, Zn) co-doping on structural, optical and bactericidal properties of CuO nanoparticles synthesized by a microwave-assisted method. *Dalton Trans.* **50**, 6188–6203 (2021). <https://doi.org/10.1039/D0DT04405A>
 33. S. Sharma, K. Kumar, N. Thakur, Green synthesis of silver nanoparticles and evaluation of their anti-bacterial activities: use of *Aloe barbadensis* miller and *Ocimum tenuiflorum* leaf extracts. *Nanofabrication* **6**, 52–67 (2021). <https://doi.org/10.1515/nanofab-2020-0102>
 34. P. Jamdagni, P. Khatri, J.S. Rana, Green synthesis of zinc oxide nanoparticles using flower extract of *Nyctanthes arbor-tristis* and their antifungal activity. *J. King Saud Univ. Sci.* **30**, 168–175 (2018). <https://doi.org/10.1016/j.jksus.2016.10.002>
 35. S. Joshi, M. Mudigere, L. Krishnamurthy, G. Shekar, Growth and morphological studies of NiO/CuO/ZnO based nanostructured thin films for photovoltaic applications. *Chem. Pap.* **68**, 1584–1592 (2014). <https://doi.org/10.2478/s11696-014-0596-9>
 36. B. Arunkumar, S.J. Jeyakumar, M. Jothibas, A sol-gel approach to the synthesis of CuO nanoparticles using *Lantana camara* leaf extract and their photo catalytic activity. *Optik* **183**, 698–705 (2019). <https://doi.org/10.1016/j.ijleo.2019.02.046>
 37. A. Muthuvel, M. Jothibas, C. Manoharan, Effect of chemically synthesis compared to biosynthesized ZnO-NPs using *Solanum nigrum* leaf extract and their photocatalytic, antibacterial and in-vitro antioxidant activity. *J. Environ. Chem. Eng.* **8**, 103705 (2020). <https://doi.org/10.1016/j.jece.2020.103705>
 38. N. Zayyoun, L. Bahmad, L. Laânab, B. Jaber, The effect of pH on the synthesis of stable Cu₂O/CuO nanoparticles by sol-gel method in a glycolic medium. *Appl. Phys. A.* **122**, 1–6 (2016). <https://doi.org/10.1007/s00339-016-0024-9>
 39. C.Y. Huang, A. Chatterjee, S.B. Liu, S.Y. Wu, C.L. Cheng, Photoluminescence properties of a single tapered CuO nanowires. *Appl. Surf. Sci.* **256**, 3688–3692 (2010). <https://doi.org/10.1016/j.apsusc.2010.01.007>
 40. D.C. Onwudiwe, O. Arijeh, H.U. Nwankwo, Plant-mediated biosynthesis of silver nanoparticles by leaf extracts of *Lasienthraafricanum* and a study of the influence of kinetic parameters. *Bull. Mater. Sci.* **40**, 129–137 (2017). <https://doi.org/10.1007/s12034-017-1362-8>
 41. M. Ponnar, C. Thangamani, P. Monisha, S.S. Gomathi, K. Pushpanathan, Influence of Ce doping on CuO nanoparticles synthesized by microwave irradiation method. *Appl. Surf. Sci.* **449**, 132–143 (2018). <https://doi.org/10.1016/j.apsusc.2018.01.126>

42. J. Jeevanandam, A. Barhoum, Y.S. Chan, A. Dufresne, M.K. Danquah, Review on nanoparticles and nanostructured materials: history, sources, toxicity and regulations. *Beilstein J. Nanotechnol.* **9**, 1050–1074 (2018)
43. L.B. Shi, P.F. Tang, W. Zhang, Y.P. Zhao, L.C. Zhang, H. Zhang, Green synthesis of CuO nanoparticles using *Cassia auriculata* leaf extract and in vitro evaluation of their biocompatibility with rheumatoid arthritis macrophages (RAW 264.7). *Trop. J. Pharm. Res.* **16**, 185–192 (2017). <https://doi.org/10.4314/tjpr.v16i1.25>
44. S.A. Gaddam, V.S. Kotakadi, D.V.R. SaiGopal, Y. SubbaRao, A. VaradaReddy, Efficient and robust biofabrication of silver nanoparticles by *cassia alata* leaf extract and their antimicrobial activity. *J. Nanostruct. Chem.* **4**, 1–9 (2014). <https://doi.org/10.1007/s40097-014-0082-5>
45. F. Buazar, S. Sweidi, M. Badri, F. Kroushawi, Biofabrication of highly pure copper oxide nanoparticles using wheat seed extract and their catalytic activity: a mechanistic approach. *Green Process. Synth.* **8**, 691–702 (2019). <https://doi.org/10.1515/gps-2019-0040>
46. C. Tamuly, I. Saikia, M. Hazarika, M.R. Das, Reduction of aromatic nitro compounds catalyzed by biogenic CuO nanoparticles. *RSC Adv.* **4**, 53229–53236 (2014). <https://doi.org/10.1039/C4RA10397A>
47. L. Yang, D. Chu, L. Wang, X. Wu, J. Luo, Synthesis and photocatalytic activity of chrysanthemum-like Cu₂O/Carbon nanotubes nanocomposites. *Ceram. Int.* **42**, 2502–2509 (2016). <https://doi.org/10.1016/j.ceramint.2015.10.051>
48. V. Lobo, A. Patil, A. Phatak, N. Chandra, Free radicals, antioxidants and functional foods: Impact on human health. *Pharmacogn. Rev.* **4**, 118 (2010). <https://doi.org/10.4103/2F0973-7847.70902>
49. C. Shanmugam, G. Sivasubramanian, B. Parthasarathi, K. Baskaran, R. Balachander, V.R. Parameswaran, Antimicrobial, free radical scavenging activities and catalytic oxidation of benzyl alcohol by nano-silver synthesized from the leaf extract of *Aristolochia indica* L: a promenade towards sustainability. *Appl. Nanosci.* **6**, 711–723 (2016). <https://doi.org/10.1007/s13204-015-0477-8>
50. B. Siripireddy, B.K. Mandal, Facile green synthesis of zinc oxide nanoparticles by *Eucalyptus globulus* and their photocatalytic and antioxidant activity. *Adv. Powder Technol.* **28**, 785–797 (2017). <https://doi.org/10.1016/j.apt.2016.11.026>
51. G.K. Prashanth, P.A. Prashanth, U. Bora, M. Gadewar, B.M. Nagabhushana, S. Ananda, G.M. Krishnaiah, H.M. Sathyananda, In vitro antibacterial and cytotoxicity studies of ZnO nanopowders prepared by combustion assisted facile green synthesis. *Karbala Int. J. Mod. Sci.* **1**, 67–77 (2015). <https://doi.org/10.1016/j.kijoms.2015.10.007>
52. S.H. Amirmordin, H.A. Rahman, H.Z. Abdullah, H. Taib, Effect of zeta potential of stannum oxide (SnO₂) on electrophoretic deposition (EPD) on porous alumina. In *Adv. Mater. Res.* **795**, 334–337 (2013). <https://doi.org/10.4028/www.scientific.net/AMR.795.334>
53. N. Thakur, K. Kumar, V.K. Thakur, S. Soni, A. Kumar, S.S. Samant, Antibacterial and photocatalytic activity of undoped and (Ag, Fe) co-doped CuO nanoparticles via microwave-assisted method. *Nanofabrication* (2022). <https://doi.org/10.37819/nanofab.007.186>
54. N. Thakur, N. Thakur, V. Bhullar, S. Sharma, A. Mahajan, K. Kumar, D.P. Sharma, D. Pathak, TiO₂ nanofibers fabricated by electrospinning technique and degradation of MO dye under UV light. *Z. für Krist.—Cryst. Mater.* **236**, 239–250 (2021). <https://doi.org/10.1515/zkri-2021-2025>
55. Z. Thammavongsy, I.P. Mercer, J.Y. Yang, Promoting proton coupled electron transfer in redox catalysts through molecular design. *Chem. Commun.* **55**, 10342–10358 (2019). <https://doi.org/10.1039/C9CC90334H>
56. M. Velayati, H. Hassani, Z. Sabouri, A. Mostafapour, M. Darroudi, Biosynthesis of Se-Nanorods using Gum Arabic (GA) and investigation of their photocatalytic and cytotoxicity effects. *Inorg. Chem. Commun.* **128**, 108589 (2021). <https://doi.org/10.1016/j.inoche.2021.108589>
57. D. Paul, S. Neogi, Synthesis, characterization and a comparative antibacterial study of CuO, NiO and CuO-NiO mixed metal oxide. *Mater. Res. Express.* **6**, 1–15 (2019). <https://doi.org/10.1088/2053-1591/ab003c>
58. S. Sharma, K. Kumar, N. Thakur, M.S. Chauhan, *Ocimum tenuiflorum* leaf extract as a green mediator for the synthesis of ZnO nanocapsules inactivating bacterial pathogens. *Chem. Pap.* **74**, 3431–3444 (2020). <https://doi.org/10.1007/s11696-020-01177-3>
59. S. Qiu, H. Zhou, Z. Shen, L. Hao, H. Chen, X. Zhou, Synthesis, characterization, and comparison of antibacterial effects and elucidating the mechanism of ZnO, CuO and CuZnO nanoparticles supported on mesoporous silica SBA-3. *RSC Adv.* **10**, 2767–2785 (2020). <https://doi.org/10.1039/c9ra09829a>
60. K.S. Siddiqi, A. Husen, R.A.K. Rao, A review on biosynthesis of silver nanoparticles and their biocidal properties. *J. Nanobiotechnol.* **16**, 14 (2018). <https://doi.org/10.1186/s12951-018-0334-5>
61. D.A. Pelletier, A.K. Suresh, G.A. Holton, C.K. McKeown, W. Wang, B. Gu, N.P. Mortensen, D.P. Allison, D.C. Joy, M.R. Allison, Effects of engineered cerium oxide nanoparticles on bacterial growth and viability. *Appl. Environ. Microbiol.* **76**, 7981–7989 (2010)
62. J.S. McQuillan, H. Groenaga Infante, E. Stokes, A.M. Shaw, Silver nanoparticle enhanced silver ion stress response in

- Escherichia coli* K12. *Nanotoxicology* **6**, 857–866 (2012). <https://doi.org/10.3109/17435390.2011.626532>
63. A.H. Hirad, S.A. Ansari, M.A.E. Ali, M.A. Egeh, Microwave-mediated synthesis of iron oxide nanoparticles: photocatalytic, antimicrobial and their cytotoxicity assessment. *Process Biochem.* **118**, 205–214 (2022). <https://doi.org/10.1016/j.procbio.2022.04.022>
64. A. Annapoorani, A. Koodalingam, M. Beulaja, G. Saiprasad, P. Chitra, A. Stephen, S. Palanisamy, N.M. Prabhu, S. You, S. Janarthanan, R. Manikandan, Eco-friendly synthesis of zinc oxide nanoparticles using *Rivina humilis* leaf extract and their biomedical applications. *Process Biochem.* **112**, 192–202 (2022). <https://doi.org/10.1016/j.procbio.2021.11.022>

Publisher's Note Springer Nature remains neutral with regard to jurisdictional claims in published maps and institutional affiliations.

Springer Nature or its licensor (e.g. a society or other partner) holds exclusive rights to this article under a publishing agreement with the author(s) or other rightsholder(s); author self-archiving of the accepted manuscript version of this article is solely governed by the terms of such publishing agreement and applicable law.